ACTA METALLURGICA SLOVACA
2023, VOL. 29, NO. 3, 155-160

RESEARCH PAPER

OPTIMIZATION OF THE RFW PROCESS PARAMETERS BY USING THE TAGUCHI METHOD FOR THE Ti6Al4V GRADE-5 ALLOY

Houssem Eddine Lakache[1], Abdelghani May[1], Riad Badji[2]*

[1] Laboratoire Génie des Matériaux, École Militaire Polytechnique, BP 17, 16214, Alger, Algeria.
[2] Research Centre in Industrial Technologies (CRTI), B. P 64 Cheraga Algeria.

*Corresponding author: lakache.houssem@mail.com, tel.: (+213) 0660222376, Laboratoire Génie des Matériaux, École Militaire Polytechnique, BP 17, 16214, Alger, Algérie.

Received: 08.08.2023
Accepted: 22.09.2023

ABSTRACT

The primary goal of this study is to implement the Rotary Friction Welding (RFW) process to join similar Ti6Al4V welds. The experimental procedure involves the deliberate manipulation of input parameters, including rotational speed, friction pressure, and friction time, through the utilization of Taguchi's L9 orthogonal array methodology. This approach is facilitated using the MINITAB software to generate a visual representation of the response chart. The primary focus of the investigation centers on the assessment of the Ultimate Tensile Strength (UTS) of the welded joint, serving as the selected output parameter. The central objective is to identify the optimal RFW conditions that lead to the highest achievable UTS. Furthermore, by conducting thorough statistical analysis of variance (ANOVA), the most influential process parameter is identified and analyzed. The concluding phase involves the development of a comprehensive regression equation governing the UTS for the titanium alloy. The accuracy and reliability of this equation are then validated through rigorous experimental tests and the corresponding observed values. The highest UTS value (1040.24 MPa) was obtained by using a rotational speed of 2000 rpm, a friction pressure of 10.7 MPa, and a friction time of 7.8 s. Microscopic observations indicate the existence of three zones in the friction welded joint, each of which has a specific metallography depending on the effect it undergoes during the welding operation. The fractured surface exhibits a rough cupular morphology with numerous dimples, suggesting a ductile fracture mode.

Keywords: Taguchi; ANOVA; RFW; Ti6Al4V grade-5

INTRODUCTION

The RFW process emerges as a solid-state welding technique that harnesses heat generation through mechanical friction, juxtaposing a mobile rod against a stationary one, while employing lateral force. This process generally occurs in two distinct phases. The initial one is the friction phase, when the welding heat is generated to soften the material and elicit flash formation at the interface [1]. Subsequently, the forging phase follows, denoting the cessation of rotation coupled with augmented pressure. This phase assumes a pivotal role in consolidating and cooling the friction weld joint [2]. In the RFW process, the weld joint is formed under the viscous plasticity conditions [3]. Since RFW is a relatively new method for joining similar and dissimilar materials, little is known about its impact on mechanical characteristics of the weld joint as well as changes in microstructure at the interface [4]. Higher quality joints can be anticipated due to the RFW process's attributes, such as its short welding cycle and the extrusion of plasticized metal at the interface [5], which effectively inhibit the formation of intermetallic compounds at the joint interface [6].

Titanium is an extraordinary metal that has gained remarkable importance in a wide range of industries, owing to its distinct properties. As a result of its notable strength-to-weight ratio, impressive resistance to corrosion, and inherent biocompatibility, titanium finds versatile applications spanning aerospace, medical implants, and marine engineering [7, 8]. Solid state welding processes such as friction welding [9-10], have the potential to create high quality joints in titanium alloys by circumventing common problems such as segregation, porosity, and grain coarsening that frequently arise in fusion welding or brazing processes. RFW, in particular, has demonstrated its effectiveness in welding titanium alloys, primarily due to its lower welding temperatures and shorter welding cycles, which help to reduce residual stress and suppress metallurgical reaction [11].

The strength of the RFW joint finds intricate connections with the selection of diverse parameters encompassing rotational speed, friction and forging time, in addition to friction and forging pressure [12-14]. The optimization of these parameters remains imperative to guarantee the achievement of increased mechanical attributes within the RFW joints. By judiciously refining these variables, the global efficiency and soundness of the welded joints can experience a notable increase. The flash's shape at the macro level might yield preliminary information on the weld strength, while the estimation of the RFW joint's mechanical properties necessitates comprehensive mechanical tests.

Apart from conducting experimental investigations, novel statistical techniques were employed to ascertain the optimal parameters, aiming to minimize the number of experiments [15-16]. In this methodology, Paventhan et al. [15]. applied Response Surface Methodology (RSM) as a statistical tool to optimize the RFW process parameters, ultimately achieving the highest UTS value of the dissimilar joints between AA6082 and AISI 304 austenitic stainless steel. Mathiazhagan et al. [16] established an empirical relationship between the friction welding parameters and the tensile properties of the dissimilar AA6063/AISI

304 weld joint. They employed the Response Surface Methodology (RSM) technique in conjunction with the Adaptive Neuro-Fuzzy Inference System (ANFIS) technique. The Taguchi statistical approach emerges as a robust instrument to specify significant factors while minimizing the requisite number of tests [17]. This methodology has been harnessed by Mattie et al. [18] to fine-tune RFW welding process parameters for the dissimilar austenitic and ferritic stainless steel tubes using finite element analysis. It was found that friction time and forging pressure had the highest percentage contribution to Von-Mises stress and total deformation. Furthermore, Murugan and Rajkamal [19] used Taguchi orthogonal arrays to optimize the UTS and microhardness values of the dissimilar RFW joints (SS304 stainless steel and AA6063 aluminium), they concluded that increasing the friction pressure also increases the UTS value of dissimilar RFW joints.

Various researchers have examined the impact of each parameter in the RFW process on Ti6Al4V weld joints while keeping the remaining parameters constant [12, 20, 21]. In their study, Demouche et al. [22] found a correlation between an increase in RFW sample's UTS and the increase in friction time and pressure, although up to a specific threshold, beyond which UTS exhibited a decline.

While extensive research is documented, it becomes evident that the application of the Taguchi method to optimize RFW process parameters for the Ti6Al4V grade-5 titanium alloy remains relatively uncharted. The primary objective of this research is to identify the influences of parameters governing the RFW process. This is achieved by executing welding tests on the Ti6Al4V weld joints, ultimately resulting in an optimized model derived from these parameters. This paper is sectioned into two distinct parts. The initial one revolves around the mechanical characterization of RFW joints through meticulous tensile tests, based on a methodically experimental plan. Subsequently, the focus shifts towards refining the regression model extracted through the Taguchi method, with the aim of identifying the optimal value. The outcomes emerging from this optimization research will be comprehensively debated.

MATERIAL AND METHODS

The research is centered on the utilization of Ti6Al4V grade-5 titanium alloy as the chosen material, with its chemical composition outlined in **Table 1**. To visually document the base material, **Fig. 1** shows its optical micrograph. This figure captures the material attribute subsequent to undergoing a meticulous process involving polishing and chemical etching with a reagent composed of 1ml HF, 2ml HNO_3, and 17ml H_2O for a duration of 15 seconds. For the friction welding operations, cylindrical samples are prepared, possessing dimensions of Ø15 mm × 50 mm. Subsequent to the RFW process, samples for tensile testing are precisely machined from the resultant RFW joints, adhering to the ISO 6892-1:2016 standard. The tensile tests were conducted at 20 °C and $10^{-3}s^{-1}$ strain rate using an MTS machine. The evaluation of fracture surfaces is undertaken through examination under a ZEISS (EVO MA 25) Scanning Electron Microscope.

Table 1 Chemical composition of the Ti6Al4V alloy.

Elements	Ti	Al	V	C	Fe	Sn
wt.%	89.65	5.48	4.22	0.369	0.112	0.0725
	Nb	**Si**	**Cu**	**Cr**	**Zr**	**Ni**
	0.0386	0.022	0.020	0.0099	0.0028	<0.001

Regarding the Ti6Al4V alloy, the microstructure distinctly showcases a characteristic Ti (α + β) configuration, which is visually depicted in **Fig. 1**. This particular microstructural arrangement is attributable to the role of aluminum as an α-stabilizer and vanadium as a β-stabilizer [23]. The microstructure itself is characterized by a matrix encompassing equiaxed grains of the α phase, noted for their lighter hue. Intermingled within this matrix are grains of the darker colored β phase [24].

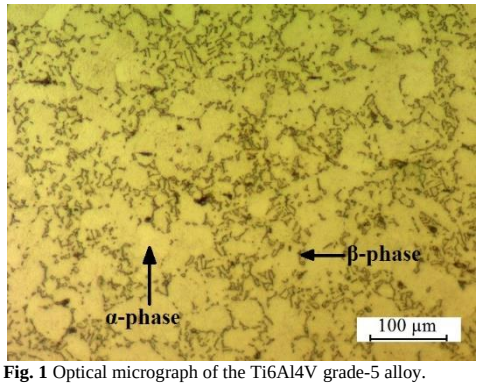

Fig. 1 Optical micrograph of the Ti6Al4V grade-5 alloy.

The RFW procedures are executed utilizing a direct drive machine responsible for overseeing welding aspects including pressure, time, and rotational speed. By combining previous friction welding tests and literature data, a range of RFW process parameters values was selected. The sequence commences with bringing the two rods into contact, a stage clearly depicted in **Fig. 2(a)**. Subsequently, in the friction phase (See **Fig. 2(b-d)**), a designated friction pressure denoted as P_1, is meticulously applied for a precisely determined duration referred to as t_1.

The heat generated at the interface between the two rods induces a state of plastic deformation within the material, leading to the formation of a toroidal-shaped flash towards the outside. The end of the friction phase corresponds with the cessation of rotational motion, signifying the beginning of the forging phase (See **Fig. 2(e)**). This phase entails the application of forging pressure, specifically identified as P_2, for a predetermined forging time denoted as t_2.

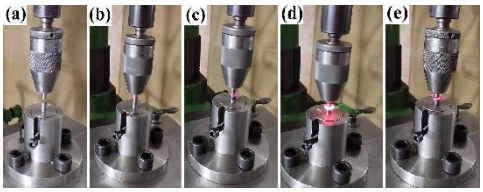

Fig. 2 RFW process phases during the welding operation: (a) accosting, (b, c and d) friction, (e) forging.

RESULT AND DISCUSSION

Optimization of the RFW parameters

During this stage, a systematically organized sequence of tests has been diligently executed, aimed at revealing the most favorable compromise of parameters that guarantees the maximization of the tensile strength within the RFW joints. The experimental data accumulated through these tests will undergo meticulous analysis in the concluding part of this section. The ensuing analysis will entail the interpretation of outcomes and the fine-tuning of the model. For the formulation of the Taguchi method, the MINITAB software was used as a statistical instrument within this investigation.

For the optimization of RFW process parameters, a trio of pivotal variables, namely rotational speed A (rpm), friction pressure B (MPa), and friction time C (s), have been designated for variation, as shown in **Table 2**. Concurrently, the other parameters are kept constant, specifically forging time (6 seconds) and forging pressure (5 MPa).

Table 2 Factors and levels.

Factor	Level 1	Level 2	Level 3
A (rpm)	1200	1600	2000
B (MPa)	4	8	12
C (s)	4	6	8

Extensive analyzes guided the selection of the examined factors, ensuring a broad range of tests that could reveal the impacts of each factor. For every factor, a trilogy of distinct levels was meticulously chosen, a selection supported by information gathered from previous experimental trials. The experiment was planned to transition from a lower level through an intermediate level, ultimately culminating at a higher level. This careful progression guarantees the precision and fidelity of the results acquired.
The Taguchi method presents an array of experimental configurations, delineated within tables, their composition reliant on the factors and their respective levels. In alignment with this study, the L9 model (3^3) was opted for, featuring nine distinct experimental iterations, by combining three levels and three factors, all meticulously depicted within **Table 3**.

Table 3 L9 orthogonal arrays with mechanical tests results.

Input parameters				
Sample	**A (rpm)**	**B (MPa)**	**C (s)**	**UTS (MPa)**
S1	1200	4	4	857.59
S2	1200	8	6	912.90
S3	1200	12	8	915.81
S4	1600	4	6	934.88
S5	1600	8	8	975.58
S6	1600	12	4	972.36
S7	2000	4	8	996.52
S8	2000	8	4	1017.75
S9	2000	12	6	1030.23

Fig. 3 shows the RFW specimens produced through the precise configuration of parameters outlined in **Table 3**. It becomes apparent that a conspicuous material deformation is observed, manifested as a flash at the weld interface. This particular occurrence arises as a consequence of the substantial mechanical exertion associated with the elevated thermal energy inherent to the RFW process, giving rise to a thermoplastic deformation.

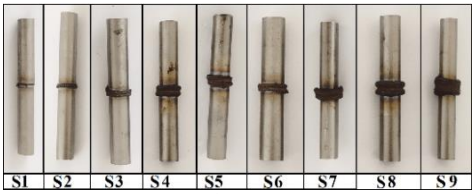

Fig. 3 Friction weld joints of the Ti6Al4V alloy.

Evaluating the mechanical characteristics of an RFW joint most often involves determining its UTS. The outcomes resulting from the conducted tensile tests are shown in **Fig. 4** and **Table 3**. For reference, a test was concurrently conducted on the titanium alloy's base metal, yielding a UTS measurement of 1037.70 MPa. Examining the fractured Ti6Al4V specimens reveals a clear presence of section necking.

Fig. 4 Fractured tensile test specimens.

The ascertained UTS values were exploited for the assessment of RFW process parameters through the application of the Taguchi methodology. Additionally, both factor responses and variance analysis were performed employing the MINITAB software.
Throughout this study, a confidence level of 95% is consistently applied. The ANOVA analysis pertinent to RFW process parameters is meticulously outlined within **Table 4**, showing the percentage contribution of each distinct parameter. The results showed that the rotation speed appears to be the predominant influencing factor, exerting a substantial impact on the UTS of the Ti6Al4V weld joint. This factor alone accounts for a notable 85.10% of the overall variability. In contrast, the friction pressure's influence is relatively weak, contributing only 13.51% to the cumulative variation. The friction time, demonstrates a marginal impact on UTS, contributing only 1.16%.

Table 4 Analysis of variance for UTS.

Source	Dof	Seq SS	Seq MS	F	P	Contribution (%)
A	2	21452.0	10726.0	356.75	0.003	85.0956
B	2	3404.5	1702.2	56.62	0.017	13.5050
C	2	292.6	146.3	4.87	0.170	1.1607
Error	2	60.1	30.1			0.2387
Total	8	25209.2				100

Employing the Taguchi approach, a loss function is exploited to quantify the disparity between experimental outcomes and the desired ones. This loss function subsequently undergoes conversion into a signal-to-noise (S/N) ratio. For each iteration of the process, the S/N ratio is computed through comprehensive S/N analysis. When analysing the S/N ratio, three distinct categories of quality characteristics emerge: "smaller the better," "larger the better," and "nominal the better." In the context of this study, the goal is the maximization of the UTS. Consequently, the "larger the better" S/N ratio is adopted and evaluated in accordance with equation (1) [25].

$$S/N = -10 * \log\left(\left(1/N\right) * \sum_{i=1}^{N}\left(1/y_i^2\right)\right) \quad (1.)$$

where: yi - The data recorded for the ith performance characteristic.
N - Total count of tests.

The findings of this assessment are presented in **Table 5**, encompassing the S/N ratios as well as the mean responses

corresponding to the UTS values. The outcomes, as derived through the Taguchi methodology, describing the optimal levels of the control factors. For a visual representation of these optimal values, graphical representations are shown in **Figs. 5 & 6**.

Table 5 Responses of the S/N ratios and the means for the factors.

	Level	A (rpm)	B (MPa)	C (s)
S/N ratio	1	59.04	59.35	59.52
	2	59.65	59.72	59.63
	3	60.13	59.75	59.66
	Delta	1.09	0.40	0.14
Mean	1	895.4	929.7	949.2
	2	960.9	968.7	959.3
	3	1014.8	972.8	962.6
	Delta	119.4	43.1	13.4
	Rank	1	2	3

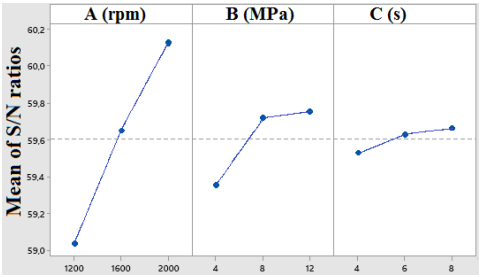

Fig. 5 Main effect plots of S/N ratios for the UTS of the Ti6Al4V weld joint.

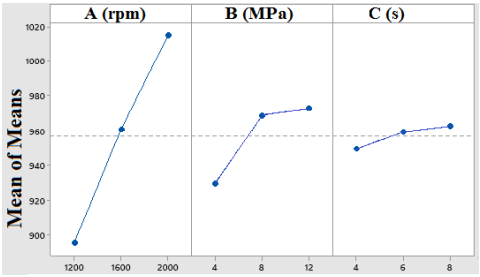

Fig. 6 Main effect plots of means for the UTS of the Ti6Al4V weld joint.

The levels and corresponding S/N ratios linked to the factors that yielded the most elevated UTS value for the Ti6Al4V weld joint were clearly defined, for factor A, Level 3 was predominant, accompanied by an S/N ratio of 60.13. Factor B has a similar pattern, with Level 3 and an S/N ratio of 59.75. Similarly, for factor C, Level 3 was predominant, with an S/N ratio of 59.66. This means that an optimum UTS value is obtained by setting the rotational speed to 2000 rpm, the friction pressure to 12 MPa and the friction time to 8 seconds.

This study positions UTS as the dependent variable, whereas the rotational speed, friction pressure, and friction time, which together serve as the independent variables. The resultant predictive equation, structured to encompass quadratic regression for the UTS value (in MPa) of the Ti6Al4V weld joint, takes the form of equation (2), which contains the variables: A in rpm, B in MPa, C in seconds.

$$UTS_p = 473.3 + 0.2654 * A + 22.9 * B + 13.6 * C - 0.000036 * A^2 - 1.094 * B^2 - 0.85 * C^2 \quad (2.)$$

Illustrated in **Fig. 7** is the juxtaposition between experimental end predicted UTS values of the Ti6Al4V weld joint, this validation curve is represented by equation (3). An evident alignment is observed with a similarity coefficient denoted as R^2 = 0.9976, signaling a great similarity between the calculated and actual UTS values.

$$UTS_p = -2 + 1.0032 * UTS_{exp} \quad (3.)$$

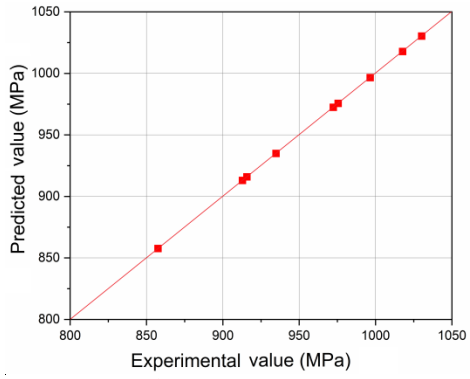

Fig. 7 Comparison of experimental end predicted UTS values.

The optimization of the UTS regression model necessitates the application of a nonlinear programming solver, serving as an optimization instrument. Within the current inquiry, the UTS regression equation unfolds as an unconstrained nonlinear function. The solver yields a UTS measurement of 1040.24 MPa, obtained by the combination of A = 2000 rpm, B = 10.7 MPa, and C = 7.8 seconds. This outcome delineates an impressive enhancement of 100.24% compared to the Ti6Al4V base metal (1037.70 MPa).

Microscopic observations

Fig. 8(a) illustrates the optical microstructure of the Ti6Al4V weld joint produced using the optimal RFW process parameters (Rotational speed of 2000 rpm, friction pressure 10.7 MPa and friction time of 7.8 s). In this figure, the α phase is evident as a lighter color within the darker β phase. The interface resulting from the friction welding displays a distinct material flow between the dynamic recrystallization zone (DRZ) and the base metal. It's worth observing that the grains in the thermo-mechanically affected zone (TMAZ) and the heat-affected zone (HAZ) have been refined (See **Figs. 8(b) & (c)**). This refinement is a consequence of the significant plastic deformation combined with the thermal effects. This phenomenon leads to the fragmentation of grains and the creation of dislocation loops. These loops accumulate at sub-grain boundaries and eventually transform into new recrystallized sub-grains, contributing to the overall grain refinement through the RFW process [26].

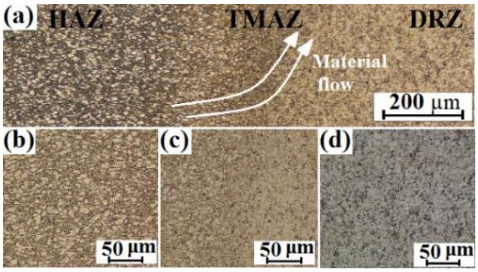

Fig. 8 (a) Optical microstructure of the weld joint, (b) HAZ, (c) TMAZ, (d) DRZ.

Several researchers [26-30] have documented that the microstructure observed in the central zone is formed as a result of dynamic recrystallization (**Figs. 8(d)**). The grains in the TMAZ adjust their orientation in response to the direction of material flow. In contrast, the HAZ only undergoes thermal cycles, and the base metal remains unaffected during the welding process. The heat produced during the RFW, combined with the substantial mechanical stress, gives rise to interdiffusion of atoms at the friction weld interface. It's important to note that the primary mechanism underlying bonding in the friction welding process is the phenomenon of atom diffusion [30]. Notably, the bonding during RFW largely depends on the material mixture, as this factor holds a pivotal role in the friction welding process [31].

Fractographic analysis

The fracture surface of the Ti6Al4V RFW specimen, which is obtained by using the previous optimal parameters, exhibits a distinct reduction in surface area when compared with the cross-sectional dimension of the tensile test specimen. This phenomenon is a direct outcome of the necking effect. Along the periphery of the fracture surface, sharp edges visibly emerge, as shown in **Fig. 9**. For enhanced visualization of the surface morphology, a focused view of the central region is presented in **Fig. 10(a)**. Within this magnified view, the morphological attributes remain uniform, where the middle region displaying a coarse texture filled with cupules, having an average diameter of 10 µm, as shown in **Fig. 10(b)**. This observation suggests a ductile mode of failure, indicating substantial plastic deformation. These findings correspond to the results published by Vikas et al. [32].

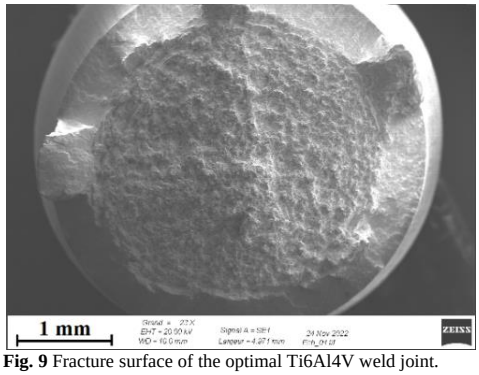

Fig. 9 Fracture surface of the optimal Ti6Al4V weld joint.

The underlying conditions of the RFW process, encompassing rotational speed, time, and pressure, exert a powerful influence on the heat generated during frictional interaction. This heightened temperature triggers a transition of the material to a semi-solid state, accelerating atom diffusion at the interface between the welded rods. This transformative process ensures changes in the microstructure through the dynamic recrystallization phenomenon of the grains [31, 33-34].

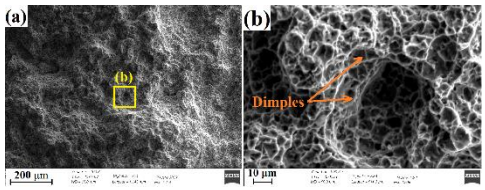

Fig. 10 (a) Morphology of the central zone of the fracture surface, (b) Magnification of the boxed area in (a).

CONCLUSIONS

The Taguchi method is used to optimize the RFW process parameters and generate a regression model that provides acceptable predicted results. The Ti6Al4V alloy's UTS demonstrates a significant responsiveness to changes in rotational speed, playing a vital role in determining the mechanical properties of the RFW joints. Meanwhile, the contribution of frictional pressure to the UTS value is only 13.51%. Conversely, friction time has a marginal impact on UTS (1.16%), which is considered a negligible effect. The greatest UTS value (1040.24 MPa) was achieved by using the parameters A = 2000 rpm, B = 10.7 MPa, and C = 7.8 s. This result represents an improvement in the UTS value of 0.24% compared to that of the base metal. The DRZ exhibits material flow near the friction weld interface, where the grains are fully recrystallized. On the other hand, the grains of TMAZ and HAZ were refined, a consequence of the combined effect of the severe plastic deformation and the thermal welding cycle. The fractured surface displays a rough cupular morphology with various dimples, indicating a ductile mode of failure.

REFERENCES

1. H. E. Lakache, A. May, R. Badji: Engineering Solid Mechanics, 11(3), 2023, 291- 298. http://dx.doi.org/10.5267/j.esm.2023.2.003.
2. W. Li, A. Vairis, M. Preuss, T. Ma: International Materials Reviews, 61(2), 2016, 71-100. https://doi.org/10.1080/09506608.2015.1109214.
3. M. A. Tashkandi, M. Gamil: Acta Metallurgica Slovaca, 28(3), 2022, 157-164. https://doi.org/10.36547/ams.28.3.1573.
4. M. Meisnar, S. Baker, J. M. Bennett, A. Bernad, A. Mostafa, S. Resch, N. Fernandes, A. Norman: Materials & Design, 132, 2017, 188-197. https://doi.org/10.1016/j.matdes.2017.07.004.
5. Z. Liang, G. Qin, L. Wang, X. Meng, F. Li: Materials Science and Engineering: A, 645, 2015, 170-180. https://doi.org/10.1016/j.msea.2015.07.089.
6. Li, J. Li, Z. Liao, F. Jin, F. Zhang, J. Xiong: Materials & Design, 99, 2016, 26-36. https://doi.org/10.1016/j.matdes.2016.03.037.
7. D. Banerjee, J. C. Williams: Acta Materialia, 61(3), 2013, 844-879. https://doi.org/10.1016/j.actamat.2012.10.043.
8. N. Hynes, P. S. Velu, A. M. Nithin: Journal of the Brazilian Society of Mechanical Sciences and Engineering, 40, 2018, 1-7.

https://doi.org/10.1007/s40430-018-1088-6.
9. M. Kimura, T. Iijima, M. Kusaka, K. Kaizu, A. Fuji: Journal of Manufacturing Processes, 24, 2016, 203-211. https://doi.org/10.1016/j.jmapro.2016.09.004.
10. A. Astarita, F. Scherillo, M. Curioni, P. Aprea, F. Impero, A. Squillace, X. Zhou: Materials and Manufacturing Processes, 31(16), 2016, 2115-2122. https://doi.org/10.1080/10426914.2016.1151048.
11. P. Li, H. Dong, Y. Xia, X. Hao, S. Wang, L. Pan, J. Zhou: Journal of Manufacturing Processes, 33, 2018, 54-63. https://doi.org/10.1016/j.jmapro.2018.05.001.
12. M. Avinash, G. V. K. Chaitanya, D. K. Giri, S. Upadhya, B. K. Muralidhara: Microstructure and mechanical behaviuor of rotary friction welded titanium alloys, In.: *Proceedings of world academy of science, engineering and technology*, 26, 2007, 1307-6884. https://doi.org/10.5281/zenodo.1078985.
13. R. Selvaraj, K. Shanmugam, P. Selvaraj, V. Balasubramanian: Forces in Mechanics, 10, 2023, 100175. https://doi.org/10.1016/j.finmec.2023.100175.
14. H. E. Lakache, A. May, R. Badji, S. E. Benhammouda, S. Ramtani: Experimental Techniques, 2023, 1-12. https://doi.org/10.1007/s40799-023-00671-z.
15. R. Paventhan, P. R. Lakshminarayanan, V. Balasubramanian: Transactions of Nonferrous Metals Society of China, 21(7), 2011, 1480-1485. https://doi.org/10.1016/S1003-6326(11)60884-4.
16. N. Mathiazhagan, T. S. Kumar, M. Chandrasekar: Asian Journal of Research in Social Sciences and Humanities, 6(8), 2016, 2089-2105. http://dx.doi.org/10.5958/2249-7315.2016.00733.4.
17. M. Koilraj, V. Sundareswaran, S. Vijayan, S. K. Rao: Materials & Design, 42, 2012, 1-7. https://doi.org/10.1016/j.matdes.2012.02.016.
18. A. A. Mattie, S. Y. Ezdeen, G. I. Khidhir: Advances in Mechanical Engineering, 15(7), 2023, 1-16. https://doi.org/10.1177/16878132231186015.
19. S. S. Murugan, S. Rajkamal: International Journal of Advanced Science and Engineering, 8(2), 2021, 2147-2152. https://doi.org/10.29294/IJASE.8.2.2021.2147-2152.
20. D. M. Mukhawana, P. M. Mashinini, D. M. Madyira: Analysis of the Microstructure and Microhardness of Rotary Friction Welded Titanium (Ti-6AL-V4) Rods, In.: Eleventh South African Conference on Computational and Applied Mechanics, 2018.
21. H. E. Lakache, A. May, R. Badji: Engineering and Applied Science Research, 50(2), 2023, 176-184. https://doi.org/10.14456/easr.2023.19.
22. M. Demouche, E. H. Ouakdi, R. Louahdi: Iranian Journal of Materials Science and Engineering, 16(3), 2019, 24-31. http://dx.doi.org/10.22068/ijmse.16.3.24.
23. S. Rossi, L. Volgare, C. Perrin-Pellegrino, C. Chassigneux, E. Dousset, M. Eyraud: Materials, 13(11), 2020, 2479. https://doi.org/10.3390/ma13112479.
24. N. Kherrouba, M. Bouabdallah, R. Badji, D. Carron, M. Amir: Materials Chemistry and Physics, 181, 2016, 462-469. https://doi.org/10.1016/j.matchemphys.2016.06.082.
25. G. Taguchi: *Introduction to quality engineering: designing quality into products and processes*, Tokyo, White Plains: Asian Productivity Organization, 1986.
26. O. Mimouni, R. Badji, A. Kouadri-David, R. Gassaa, N. Chekroun, M. Hadji: Transactions of the Indian Institute of Metals, 72, 2019, 1853-1868. https://doi.org/10.1007/s12666-019-01663-7.
27. B. Heinz, B. Skrotzki: Metallurgical and Materials Transactions B, 33, 2002, 489-498. https://doi.org/10.1007/s11663-002-0059-5.
28. J. Q. Su, T. W. Nelson, R. Mishra, M. Mahoney: Acta Materialia, 51(3), 2003, 713-729. https://doi.org/10.1016/S1359-6454(02)00449-4.
29. K. Jata, S. Semiatin: Scripta materialia,43(8), 2000, 743-749. https://doi.org/10.1016/S1359-6462(00)00480-2.
30. U. Dressler, G. Biallas, U. A. Mercado: Materials Science and Engineering: A, 526(1-2), 2009, 113-117. https://doi.org/10.1016/j.msea.2009.07.006.
31. A. Vairis, G. Papazafeiropoulos, A. M. Tsainis: Advances in Manufacturing, 4, 2016, 296-304. https://doi.org/10.1007/s40436-016-0163-4.
32. K. S. R. Vikas, K. S. Rao, G. M. Reddy, V. V. Ramana: Engineering Research Express, 4(2), 2022, 025053. https://doi.org/10.1088/2631-8695/ac7a0a.
33. N. R. J. Hynes, P. S. Velu: Journal of manufacturing processes, 32, 2018, 288-297. https://doi.org/10.1016/j.jmapro.2018.02.014.
34. E. T. Akinlabi, R. M. Mahamood: *Solid-state welding: friction and friction stir welding processes*, New York: Springer International Publishing, 2020, 1-145.